# Trends and inter-annual variability of methane emissions derived from 1979-1993 global CTM simulations

F. Dentener, M. van Weele, M. Krol, S. Houweling, P. van Velthoven

Atmos. Chem. Phys. Discuss., 2, 249–287, 2002
www.atmos-chem-phys.org/acpd/2/249/


Atmospheric Chemistry and Physics Discussions

# Trends and inter-annual variability of methane emissions derived from 1979-1993 global CTM simulations

**F. Dentener[1], M. van Weele[2], M. Krol[3], S. Houweling[4], and P. van Velthoven[2]**

[1]JRC, Institute for Environment and Sustainability, I-21020 Ispra (Va), Italy
[2]KNMI, de Bilt, the Netherlands
[3]IMAU, Utrecht University, the Netherlands
[4]MPI Biogeochemistry, Jena, Germany

Received: 6 February 2002 – Accepted: 27 February 2002 – Published: 7 March 2002

Correspondence to: F. J. Dentener (frank.dentener@jrc.it)

## Abstract

The trend and interannual variability of methane sources are derived from multi-annual simulations of tropospheric photochemistry using a 3D global chemistry-transport model. Our semi-inverse analysis uses the fifteen years (1979–1993) re-analysis of ECMWF meteorological data and annually varying including photo-chemistry, in conjunction with observed $CH_4$ concentration distributions and trends derived from the NOAA-CMDL surface stations. Dividing the world in four zonal regions, (45–90 N, 0–45 N, 0–45 S; 45–90 S) we find good agreement in each region between (top-down) calculated emission trends from model simulations and (bottom-up) estimated anthropogenic emission trends based on the EDGAR global anthropogenic emission database, which amounts for the period 1979–1993 2.7 Tg $CH_4$ $yr^{-1}$. Also the top-down determined total global methane emission compares well with the total of the bottom-up estimates. We use the difference between the bottom-up and top-down determined emission trends to calculate residual emissions. These residual emissions represent the inter-annual variability of the methane emissions. Simulations have been performed in which the year-to-year meteorology, the emissions of ozone precursor gases, and the stratospheric ozone column distribution are either varied, or kept constant. The analyses reveals that the variability of the emissions is of the order of 8 Tg $CH_4$ $yr^{-1}$, and most likely related to mid- and low-latitude wetland emissions and/or biomass burning. Indeed, a weak correlation is found between the residual emissions and regional scale temperatures.

## 1. Introduction

Atmospheric methane ($CH_4$) concentrations have more than doubled since the pre-industrial era. This increase has resulted in a radiative forcing of about 0.5 $Wm^{-2}$. Methane is therefore the most important increasing greenhouse gas after $CO_2$. During the past two decades (from 1978–1998) the globally averaged methane concentration has increased from about 1520 to 1745 ppbv (Prather et al., 2001). The rate of the



ACPD

2, 249–287, 2002

methane increase has varied substantially during this period. Values were of the order of 20 ppbv $yr^{-1}$ during the 1970s, a rather constant value of 12 ppbv $yr^{-1}$ in the 1980s, and almost zero increase in the years 1992 and 1993 (Lelieveld et al., 1998; Dlugokencky et al., 1998). Over the period 1993 to 1998 the rate of increase was about 5 ppbv $yr^{-1}$.

A remarkable depression of the methane growth rate occurred during 1992 and 1993, which can with large certainty be attributed to the impact of the eruption of Mt. Pinatubo in June 1991. This eruption has likely caused lower northern latitude wetland emissions (Hogan and Harriss, 1994) and changes in the tropospheric OH content related to stratospheric ozone depletion (e.g. Bekki et al., 1994). The Pinatubo eruption clearly showed that the observed methane growth rate and its variations are the result of an imbalance between methane emissions (sources) and destruction rates (sinks).

This work attempts to assess the trend and inter-annual variability of methane emissions over the period 1979–1993 by applying a global three-dimensional chemistry transport model (CTM) combined with a combined data assimilation-mass balance approach. As an a priori estimate the model uses the natural and anthropogenic $CH_4$ emissions evaluated by Houweling et al. (1999), see Table 1. These emissions do not contain inter-annual variability. The effective $CH_4$ emissions are calculated from simulations in which the $CH_4$ observations from the NOAA CMDL network are assimilated into the model. We use the results of a set of simulations used previously to study the trends and variability of ozone ($O_3$) during the same time period (Lelieveld and Dentener, 2000). Here the simulations (including meteorological and photochemical variability) are used to investigate whether (top-down) model calculated $CH_4$ emissions and derived trends are consistent with current (bottom-up) knowledge on the temporal and spatial changes in the anthropogenic and/or natural methane sources.

Bottom-up estimates of the global methane source strength over the past two decades amount to about 500–600 Tg $CH_4$ $yr^{-1}$ (Prather et al., 2001). Extensive overviews on individual methane sources are presented in, e.g. Lelieveld et al. (1998). Natural



ACPD
2, 249–287, 2002

sources consist of high and low latitude wetlands, termites, wild animals, oceans, volcanoes and wildfires. Houweling et al. (2000) evaluated the (pre-industrial) annual wetland emissions to be between 130–194 Tg $CH_4$, all other natural sources amounting to about 40–70 Tg. Anthropogenic sources are related to production and consumption of gas and oil, ruminants, landfills, rice agriculture and biomass burning. Most bottom-up estimates of the global anthropogenic sources are remarkably similar and amount to 315–350 Tg $CH_4$ $yr^{-1}$ (Prather et al., 2001, and references therein).

The estimates of various authors of the latitudinal distributions of the emissions are more different. For example, an early study by Fung et al. (1991) distributes the anthropogenic and natural emissions over the Northern and Southern Hemisphere (NH and SH) by a ratio 499 to 144 Tg $CH_4$ $yr^{-1}$. Lelieveld et al. (1998) suggest a NH–SH ratio of 399 to 123 Tg $CH_4$ $yr^{-1}$. The inverse model results of Hein et al. (1997) indicate a ratio of 416 to 162 Tg $yr^{-1}$, whereas the adjoint inverse model of Houweling et al. (1999) rather calculates 340 and 165 Tg $CH_4$ $yr^{-1}$, for the NH and SH, respectively. Therefore, there are large uncertainties associated with the individual sources of methane and their geographical and temporal distribution.

What do we know about emission trends? Recently, Dlugokencky et al. (1998) analysed the NOAA CMDL $CH_4$ measurements for the period 1984–1996. They suggested that during this period $CH_4$ emissions must have remained almost constant. However, this conclusion strongly depends on the assumption that the global hydroxyl (OH) radical concentrations also remained constant. At present, this topic is strongly under debate. Prinn et al. (1995) and Prinn and Huang (2001) used methyl-chloroform (MCF) observations to derive an OH trend of 0.0% ± 0.2% per year for the period 1978–1993. In contrast, using the same observational data-set, but a different statistical analysis technique and assumptions on initial pre-1978 conditions, Krol et al. (1998) and Krol et al. (2001) derive a positive OH trend of 0.46 ± 0.6% per year. The latter trend estimate is more consistent with the results of the simulations used in this study as well as an independent model study by Karlsdottir et al. (2000). In a recent study Prinn et al. (2001) derive a strong positive OH trend for the period 1979–1989 followed by a

negative trend in the period 1990–2000.

The global bottom-up estimate of 500–600 Tg $CH_4$ $yr^{-1}$ is roughly consistent with top-down model estimates on the global methane source where global OH is calibrated using observed MCF concentrations (Houweling et al., 2000). However, these top-down estimates are also associated with large uncertainties of at least 10% (see Sect. 5). In addition, due to the scarcity of measurements it seems at present not possible to determine from the surface data one unique source/sink configuration (Hein et al., 1997; Fung et al., 1991). In future the availability of isotopic data may help to improve the situation (e.g. Lassey et al., 1993). Also upcoming satellite data measuring tropospheric methane columns may improve our knowledge on the geographical and temporal variation of methane sources. This work does not aim to improve the knowledge on the $CH_4$ source distributions and strengths, but rather focuses on emission variability and trends.

The CTM used in this study is described in Sect. 2. Details on the methodology to derive the emission trends for the period 1979–1993 are given in Sect. 3. This period was chosen, since we have a consistent meteorological dataset from the ECMWF-ERA15 dataset, as well as an emission dataset for this period. In Sect. 4 we will present results for 3 different simulations with different combinations of varying meteorology, emissions and stratospheric ozone boundary conditions. The sensitivity of the method to possible measurement and model errors will be discussed in Sect. 5. Conclusions are presented in Sect. 6.

## 2. Global chemistry transport model

The global chemistry-transport model TM3 (Heimann, 1995; Houweling et al., 1998; Lelieveld and Dentener, 2000, and references therein) is used in this study at a spatial resolution of 10° longitude and 7.5° latitude with 19 vertical layers. Six-hourly meteorological fields from the ECMWF (European Centre for Medium Range Weather Forecast) ERA15 re-analysis for the years 1979–1993 (Gibson et al., 1997) are utilised.

These fields include global distributions for horizontal wind, surface pressure, temperature, humidity, liquid water content, ice water content, cloud cover, large-scale and convective precipitation. Tracer advection is simulated with the so-called 'slopes' scheme Russel and Lerner (1996). Convective tracer transport is calculated with a mass flux scheme that accounts for shallow, mid-level and deep convection (Tiedtke, 1996). Turbulent vertical transport is calculated by stability dependent vertical diffusion Louis (1996). A detailed comparison between simulated and measured $Rn^{222}$ has indicated that the synoptic scale model transport properties are represented relatively accurately at the applied resolution (Dentener et al., 1999). Also the comparison between modelled ozone and several background ozone soundings as presented in Lelieveld and Dentener (2000), revealed a quite satisfactory agreement between model and measurements.

The chemical scheme is based on a modified version of CBM4 that describes the chemistry of $CH_4$-CO-NMHC-$NO_x$ (Houweling et al., 1998) as well as $NH_x$, DMS, $SO_x$ (Dentener and Crutzen, 1994). In its present form the scheme accounts for 24 photodissociation and 67 thermal reactions as well as reactions on aerosols and in clouds. Dry deposition of gases and aerosols is parameterized according to Ganzeveld et al. (1998), and wet deposition according to Guelle et al. (1998). Photolysis frequencies are calculated with the scheme by Landgraf and Crutzen (1998), including the effects of clouds, surface albedo and the overhead ozone column following Krol et al. (1998).

Stratospheric boundary conditions are applied to ozone, methane and nitric acid ($HNO_3$). At levels above 50 hPa stratospheric ozone is relaxed towards the zonal and monthly mean ozone column measurements by the Total Ozone Mapping Spectrometer (TOMS) (**?**) using a vertical distribution from an ozone climatology representative for the 1980s (Fortuin and Kelder, 1998). The ozone column above 10 hPa is prescribed. The 3D ozone variability in the stratosphere is maintained by simulated transport. Since TOMS measurements are not available for a large part of the year 1993, we apply the 1992 TOMS measurements for 1993.

$CH_4$ is destroyed mainly by OH in the troposphere and by reactions with OH, Cl

and $O^1D$ in the stratosphere. Since TM3 does not explicitly consider stratospheric reactions, we apply in the stratosphere a methane loss rate varying between 38 and 42 Tg $yr^{-1}$, based on 2D model results of Bruhl and Crutzen (1994).

Except for methane (see Sect. 3), yearly anthropogenic emissions of $NO_x$, CO, NMHC, $SO_x$, and $NH_3$ are directly taken from the emission database developed by van Aardenne et al. (2001). This database, which is based on the widely used EDGAR emission database (Olivier et al., 1999), describes the development of emissions during the period 1890–1990. We used the base years 1970, 1980, 1985, and 1990, and linearly interpolated the results for the years 1979–1990. Emissions for the period 1991–1993 are obtained by extrapolation of the 1990 emission using $CO_2$ emission statistics obtained from Marland et al. (2000). Natural emissions of $O_3$ precursor gases are prescribed as described in (Houweling et al., 1998). The emission data-set does not account for their possible inter-annual variability, with the exception of $NO_x$ resulting from lightning discharges, which is coupled to modelled convection, and therefore lightning $NO_x$ emissions show an annual variability of about 0.5 TgN $yr^{-1}$.

## 3. Analysis method

As a starting point of the simulations we use the a priori natural and anthropogenic $CH_4$ emissions that were obtained from Houweling et al. (1999), see Table 1. The anthropogenic part of these emissions, is with some small adaptations, consistent with the emissions from the EDGAR database (see below). Note that these a priori emissions do not contain inter-annual variability, and are not representative for a specific year. In a next step the measured concentrations are assimilated in the model using the measurements of the NOAA CMDL network. In order to interpret the methane trends and to determine the inter-annual variability and trend of the methane emissions we calculate so called 'natural residual emissions'. These residual emissions are calculated from the difference of the top-down determined yearly methane emissions from a model simulation constrained by observed trends, and the bottom-up estimated time

evolution of anthropogenic methane emissions from the EDGAR inventory. In this section we present the time evolution in the emission inventories and explain our method to calculate emissions from a model simulation and to derive the residual emissions.

### 3.1. Time evolution of anthropogenic emissions

In Fig. 1 we present the bottom-up estimated yearly anthropogenic methane emissions for the period 1979–1993 as adopted from van Aardenne et al. (2001). For clarity we have aggregated the detailed 1 × 1 degree data set in four zonal regions (45 N–90 N; 0–45 N; 0–45 S; 45 S–90 S) and three source categories (fossil fuel, biogenic and biomass burning). For comparison (Houweling et al., 2000), used in his study emissions of 73.4, 234.5 and 63.4, and 0.7 Tg $CH_4$ $yr^{-1}$ for the anthropogenic emissions in the 4 regions, respectively. Natural emissions (including uptake by soils) were 27.4, 56.4, 74.5 and 1.2 Tg $CH_4$ $yr^{-1}$, respectively (see Table 1). Since there are no significant anthropogenic emissions south of 45 S this region is not included separately in Fig. 1. The fossil fuel emissions encompass all emissions associated with the production and consumption of fossil fuels. Biogenic emissions contain emissions from ruminants, rice-paddies and landfills. Biomass burning emissions include savannah fires, deforestation, waste burning and domestic biogenic fuel use. At middle and high northern latitudes fossil fuel and biogenic emissions are of equal importance. At low latitudes and in the Southern Hemisphere biogenic emissions are largest. Although especially biomass burning is known to exhibit a strong inter-annual variation, such variations in anthropogenic emissions, other than by economical and demographic developments, are not taken into account in the bottom-up emission estimates. Calculated anthropogenic trends are markedly different in the mid-and-high-latitude Northern Hemisphere, and the rest of the world.

### 3.2. Boundary conditions for top-down emission estimations

For the top-down determination of the methane emissions we performed model simulations covering the period 1979 to 1993. In these simulations the calculated methane mixing ratios are adjusted in the boundary layer, i.e. the first 3 model layers up to 600 m height, using a relaxation time scale of 10 days, to match the model zonal average to a prescribed set of zonally and monthly averaged methane mixing ratios derived from observations. The choice to adjust these three model layers, rather than only the surface layer with a thickness of about 60 m, is motivated by the fact that the observational (mostly marine) data-set is probably more representative for a mixed boundary layer than for continental surface layer concentrations. The observational data set consists of the independently determined zonally and monthly averaged methane mixing ratios for the year 1987 adopted from the inverse modelling study by Hein et al. (1997), and super-imposed on this field, an annual trend. For the period 1984–1993 this trend is derived from twelve background stations from the NOAA network for which there is a complete record during this time period (see Table 2). For the period 1979–1983 we use the observed trends evaluated by Etheridge et al. (1998). By using the observed trends in combination with a zonal distribution, the main temporal and latitudinal features of the methane boundary conditions are well represented in the simulations, as shown in Fig. 2. The gradual increase of methane between 1979 and 1991 is included, as well as the smaller increases in 1992 and 1993 (see Introduction). In general the thus derived methane trends showed a good agreement with the individual station data.

### 3.3. Natural residual emissions

The following method is used to calculate the natural residual emissions ($E'$). Consider the temporal evolution of methane mixing ratio $X$ at a specific longitude, latitude and

height ($i, j, k_{1,3}$):

$$\frac{dX_{i,j,k}}{dt} = F_{i,j,k} + G(X_{zon,j,k} - X_{obs,j}). \quad (1)$$

where $F$ represents the concentration changes in the model due to emissions, transport and chemical loss at each gridpoint, and $G$ the nudging time constant (0.1 day$^{-1}$). Integration of the second part on the right of Eq. (1) over one year and converting this term to mass units using a factor $M$ yields the yearly emissions or sinks ($dE$) which need to be added to (or subtracted from) the model, in addition to the a priori natural and anthropogenic emissions, to force the model to its boundary conditions:

$$dE = \int_{t}^{t+dt} GM_{j,k}(X_{zon,j,k} - X_{obs,j})dt \quad (2)$$

Note again that as an a priori estimate we used the emissions from Houweling et al. (1999), that did not contain inter-annual variations. To calculate the natural residual emissions variability ($dE'$) we remove the anthropogenic emission trend, by subtracting from $dE$ the difference between the bottom-up determined anthropogenic emission ($E_{\text{edgar}}$) relative to its average over the 1979–1993 time period.

$$E' = dE - E_{\text{Edgar}} + \overline{E_{\text{Edgar},1979-1993}} \quad (3)$$

The residual emission variability may still contain a trend, that was not taken into account in the original bottom-up estimate. Note that this residual trend is not necessarily only 'natural': it could also be a trend which was not represented in the EDGAR database (van Aardenne et al., 2001).

A crucial assumption in our calculation of residual emissions is that the applied surface measurements and trends in the simulations are considered to be representative for larger atmospheric compartments, i.e. as zonal average and for the whole boundary layer. This is valid in first order because the monthly average measurements represent 'clean' background conditions. The representation problems connected with the use

of surface network observations have been previously discussed by Houweling et al. (2000). To assess the accuracy of our method we present in Appendix 1 a sensitivity study in which we used a synthetic annually varying emission set to calculate the residual emissions.

In the following section we present the results integrated over four regions spanning from 90 N–45 N, 45 N-Equator, Equator-45 S, and 45 S–90 S. These large regions were chosen since we expect that the errors associated with our method start dominating the results when much smaller regions are used to present the results.

## 4. Results

For the top-down determination of the methane emissions we performed three simulations covering the ERA15 period (1979–1993), and also some sensitivity studies. The three basic simulations differ such that we can assess the individual influences on the interannual variability of methane emissions of the prescribed meteorology, and the emission changes (of e.g. $NO_x$ and other precursor gases), and the stratospheric ozone column changes over this time period.

In the base simulation (S1) all three influences varied with time. This simulation has been used in previous analyses of the ozone budget as described by Lelieveld and Dentener (2000) and Peters et al. (2001). Both studies showed that ozone was realistically represented at various background locations, and a clear correlation of tropical ozone with the ENSO index was found, in good agreement with an earlier analysis of satellite observations (Ziemke et al., 1999). In a next step the monthly averaged OH fields associated with S1 were stored and used in further simulations. We verified that the use of the monthly averaged OH fields had marginal influence on our methane source calculations. In the second simulation (S2) meteorology was varied for the period 1979–1993 while the OH fields from S1 for the year 1987 were used. The third simulation (S3) uses one repeated meteorological year (1987), while OH for the period 1979–1993 derived from S1 was used. Thus, all three simulations had the year



ACPD
2, 249–287, 2002

1987 in common, which can be used to detect possible discrepancies among the simulations. Further, the 3 simulations show the role of chemistry (OH) versus transport. More simulations would be needed to determine the separate roles of sources, boundary conditions, and meteorological parameters such as water vapor and temperature. In all cases the model used the data-assimilation procedure for methane as explained in the previous section. All simulations used the a-priori methane emissions derived from Houweling et al. (1999), and used a spin-up period of two years (1977–1978). It should be noted that the largest time-scale associated with the equilibration of $CH_4$ corresponds to about 13 years (Wild and Prather, 1996), which is even larger than the tropospheric methane lifetime of about 9 years. However, using our assimilation method, such long simulations can be avoided, and the spin-up time is sufficient to account for hemispheric mixing and tropospheric-stratospheric exchange.

We start our analysis by assessing by how much and by which mechanism in our simulations the methane destruction rates have varied. In Fig. 3 we show the tropospheric lifetime of methane calculated for the reference simulation (S1) as well as the two sensitivity simulations (S2, S3). The lifetimes are calculated as the quotient of the annual average tropospheric burden and the destruction rates of $CH_4$ by OH. In this analysis a fixed tropopause of 100 hPa was used to define the tropospheric compartment. Calculated lifetimes are about 28 and 55 years in the NH and SH high latitude regions, respectively, and 6.5 years and 7.5 years for the 45 N–0 and 0–45 S latitude regions. For the period 1979–1993, our simulations indicate a clear decrease of methane lifetimes in all four regions by −0.23% to −0.36% per year (Table 3). Globally, the calculated tropospheric methane lifetime decreases from 9.2 to 8.9 years ($-0.26 \pm 0.06$% per year). This lifetime can be compared with a range of 6.5–9.8 Tg $yr^{-1}$ evaluated by Prather et al. (2001), although the comparison is rendered somewhat difficult due to differences in calculation methods (e.g. the tropopause height). Considering a somewhat shorter period (1979–1991), thus largely excluding the effect of the eruption of Mt. Pinatubo, the calculated global $CH_4$ trend is $-0.37 \pm 0.08$% $yr^{-1}$. Over the full time period our calculated OH trend, weighted to $CH_4$ destruction, is +0.26% ± 0.06 $yr^{-1}$,

which is somewhat smaller than the OH trend of 0.46% ± 0.6% $yr^{-1}$ derived by Krol et al. (1998). The standard deviations in the calculated trends are large, indicating substantial inter-annual variability due to variability in meteorology (e.g. circulation patterns, convection) and variability in the chemical boundary conditions. Our analysis shows that most of the decrease in $CH_4$ lifetime in SH high latitude regions can be attributed to the influence of stratospheric ozone decline on photolysis rates and the associated enhanced OH production. Figure 3 clearly shows that the combined influence of emissions and stratospheric ozone is determining most of the variability in the $CH_4$ lifetime. Variability due to changing transport plays a smaller but not negligible role. The change in $CH_4$ lifetime in the tropical regions is consistent with the strong increase of $NO_x$ emissions in developing countries from 1979–1993. These increases amounted, e.g. in East Asia, China, and India to 70% , 75% and 55%, respectively (van Aardenne et al., 2001). Indeed a high sensitivity of the location of $NO_x$ emissions on $CH_4$ lifetime was calculated by another model study (Gupta et al., 1998).

In Fig. 4 we present the calculated annual methane emissions for the four regions and the corresponding global total for the base run (S1). The calculated methane emissions increased from 500 Tg to 550 Tg $yr^{-1}$ during the period 1979–1991, but dropped by about 13 Tg $yr^{-1}$ to 530 Tg $yr^{-1}$ between 1991 and 1993. The calculated emissions are remarkably close to the a priori emissions of 523 Tg $yr^{-1}$ for 1987 by Houweling et al. (2000). As expected the largest methane emissions are found in the low latitude zonal regions. However, since the area represented by the 45 N-Equator region is twice as large as that from the 90 N–45 N region, the area weighted emissions in the two regions is rather similar.

In Fig. 5 we present the residual emissions, i.e. the emission changes corrected for the anthropogenic trend using the Edgar database (Eq. 3). Note that for clarity the 1987 residual emissions are taken to be 0. Table 4 gives the standard deviations and trend-estimates corresponding to Fig. 5, and considering the full period 1979–1993 and also the shorter period 1979–1991.

From Fig. 5, and in comparison with Fig. 4, it is clear that most of the year-to-year



ACPD
2, 249–287, 2002

changes in $CH_4$ emissions are due to increasing anthropogenic emissions, which are adequately accounted for in the EDGAR emission database. The negative residual trend in the 0–45 N zonal region is strongly determined by the decrease in emissions in the year 1992 and 1993. The decrease is about 13 Tg $CH_4$ per year and is likely associated with the Mt. Pinatubo volcanic eruption. For the shorter analysis period there is no significant residual trend. In the SH the model calculates a statistical significant residual trend of about 0.65 ± 0.23 Tg $CH_4$ $yr^{-1}$. However, this estimate is very uncertain because there are only 3 measurement sites available in the SH, which cover the entire period. Globally the emissions are consistent with the EDGAR database. The inter-annual variability of the global emissions amounts to about 8 Tg $yr^{-1}$. In the discussion section we will show that the real variability is probably higher.

Figure 6 presents, similar to Fig. 5, the global residual emissions calculated for the base simulation S1 and the two sensitivity studies S2 and S3. The common simulation year is 1987 and indeed similar residual emissions are calculated for this year.

The three simulations show rather similar calculated residual emissions. This shows that the applied measurements have the largest impact on the calculated residual emissions, and not the assumptions in the model simulations such as on $CH_4$ emissions, OH distribution and transport. For example, the use of 1987 OH fields (S3) does not change very much the calculated residual emissions for 1992 and 1993. This strengthens our conclusion that, integrated over the globe, the eruption of Mt. Pinatubo has lead to about 13 Tg $yr^{-1}$ $CH_4$ lower emissions in the years 1992 and 1993.

Simulation S2 with 1987 OH and varying meteorology shows a significant difference with base simulation S1 during the first years, indicating the influence of OH, the differences become small after 1987.

Comparison of simulation S3 with fixed meteorology with the base run S1 shows to what extent the year-to-year meteorological variability (transport, water vapor, temperature) influences the derived $CH_4$ emissions. The transport variability mainly involves differences in methane concentrations due to differences in large-scale transport and convection. Inter-annual variability in methane destruction is mainly caused by changes in



ACPD
2, 249–287, 2002

the transport efficiency of photo-oxidant precursor gases and by inter-annual variations of water vapor and temperature. Both types of variability have considerable effect on the OH distribution, but less on the calculated residual emissions.

To assess whether the derived emission variability correlates with meteorology, we performed a simple analysis of the correlation of the residual emissions in the four regions considered in this study and the annual average temperature variations in 12 world regions. The world regions (e.g. Africa, OECD Europe) are defined as in van Aardenne et al. (2001), and pertain only to land-surfaces. Annual average continental temperatures are derived from the ECMWF re-analysis data. Table 5 gives a cross-correlation matrix for the analysis periods 1979–1993, respectively. Only for a few regions statistically significant but weak correlations were found. Figure 7 presents for 2 regions with a correlation larger than $r = 0.6$ ($P = 0.98$), the emission-temperature relationships. The correlation between the Africa-yearly averaged temperature and the 0–45 S residual emission amounts to $r = 0.62$, and is marked by relatively elevated emissions and high temperatures in the years 1984, 1987 and 1990, and relatively low emissions in 1986, 1989, and 1992. Much of the correlation is determined by the large temperature and emission depression in 1992 and 1993, and to a lesser extent to the correlation in the years 1983, 1985, 1988, and 1990. A similar result is found for the region East Asia and 0–45 S emissions.

To assess if a physical relation may explain the correlation between the African and South East Asian yearly-averaged temperature and the emission variability, we calculate an order of magnitude estimate of the methane emission sensitivity to temperature.

We found an emission-temperature sensitivity of roughly 10 Tg $yr^{-1}K^{-1}$. Note that we assumed in this estimate that Africa and South East Asia are the dominant contributors to emission variability in the 0–45 S latitude band.

If this emission variability could be attributed to natural wetland emissions we calculate relative to wetland emissions derived for these regions (about 65 Tg $yr^{-1}$, see Table 1), a sensitivity of about 15% $K^{-1}$. Based on a process model, Walter and Heimann (2000) found a somewhat higher temperature sensitivity of methane wetland emissions



ACPD
2, 249–287, 2002

(about 20% $K^{-1}$).

Another methane source that is known to exhibit a strong inter-annual variability is biomass burning. Attribution of the 10 Tg $yr^{-1}$ emission variability fully to biomass burning (i.e. savanna burning, waste burning and deforestation) would imply an inter-annual variability of about 50%. Although certainly interannual variability of burning can be large (especially in smaller regions) it is unlikely that integrated over a larger area the interannual burning variability amounts to 50%.

## 5. Discussion

The top-down calculated emissions, trends and variability, are subject to a number of uncertainties.

Without doubt the largest uncertainty pertaining to our method is whether a prescribed zonal field for a single year modified with a trend derived from a limited set of measurements can be used to retrieve trends in emissions and to deduce variability. To estimate the uncertainty we present in the Appendix a test with prescribed emissions, which indicates that the trends of emissions can be determined with accuracy better than 50% .

Other important uncertainties result from the OH fields that are used. Our emission estimates are obtained using OH fields, which are calculated on-line within the model. Thus, these OH fields are not, as is commonly done, calibrated to give an optimized sink for methyl chloroform. Nevertheless, the calculated global emissions of 500–550 Tg $yr^{-1}$ are consistent with the range of net emissions (including a soil sink) derived by Houweling et al. (2000), i.e. 479–528 Tg $yr^{-1}$ based on a methylchloroform (MCF) calibrated OH field. However, the calibration of OH with MCF is also associated with uncertainties. For example, the uncertainty listed by (Sander et al., 2000) for the reaction between MCF and OH is 10% , although the uncertainty of this reaction relative to the reaction between OH and $CH_4$ may be less. Further, the uncertainty of the absolute calibration of MCF is about 5% (Prinn et al., 1995). It is also generally assumed

that emissions of MCF are accurate within about 1% (e.g. McCulloch and Midgley, 1996). There is however no independent test to verify this rather low uncertainty. The stratospheric and oceanic loss rates of MCF are not well determined, which may lead to systematic errors of 1–2% (Hein et al., 1997). Houweling et al. (2000) suggest that the methyl-chloroform lifetimes determined by chemical-transport models strongly depend on the model inter-hemispheric exchange times, which can be erroneous by 10% . Therefore we argue that an uncertainty of at least 10% is associated with these top-down determined global source strength of methane. In view of the uncertainties involved with the MCF calibration, which are at least 10%, a calibration of OH does not add much value to our study. We realize that the fact that we are calculating the approximately correct OH fields, without performing any calibration, might be rather fortuitous. To our experience, changes in emissions, rate constants or removal processes, within their limit of uncertainty, may easily cause differences in global OH of the order 10% or larger.

Further, except for a small trend related to population increase, our model simulations did not include inter-annual variability of biomass burning on, e.g. $NO_x$ and CO emissions. These emissions may in turn influence regional ozone and OH abundance. To give some indication on the sensitivity of our model to biomass burning $NO_x$ emissions we make a comparison with the trend resulting from anthropogenic $NO_x$ emissons. In the tropical regions from 1979–1993 these emissions may have increased by about 4.8 Tg N leading to a corresponding integrated increase of OH (weighted to $CH_4$) destruction rates) over this period by about 4% . In comparison Gupta et al. (1998) found a similar sensitivity of about 3% for an additional 5 Tg $NO_x$ emitted in the tropics. The continent with the largest biomass burning emissions is Africa. $NO_x$ emissions from savannah burning in Africa are about 2 Tg (Marufu et al., 2000). Barbosa et al. (1994) used 6 years of AVHRR data to estimate the burned area in Africa. Their lower estimate of $NO_x$ emissions is 2.8 ± 0.75 Tg $Nyr^{-1}$ Thus assuming an annual variability of these emissions for whole Africa of 25% , the corresponding influence on integrated tropical OH would be about 0.4% $yr^{-1}$ (corresponding to ca. 2 Tg $CH_4$ emis-



ACPD
2, 249–287, 2002

sion $yr^{-1}$). This is probably an upper estimate for the $NO_x$-OH-$CH_4$ sensitivity, since these emissions occur predominantly during a limited time in the dry season and under very stable conditions. Therefore this relatively low influence of $NO_x$ emission variability on methane concentrations would not alter our conclusions. However if the $NO_x$ emissions would be significantly higher, or the chemistry would be significantly different from that in other regions, this could alter our conclusions. Several research efforts by our as well as other groups are now underway to quantify inter-annual variability of biomass burning emissions and the resulting effect on photo-chemistry.

Further, it is still questionable whether or not an OH trend is present in the considered time period. Recently, there has been a lengthy discussion between Krol et al. (2001) and Prinn and Huang (2001), also see the Introduction. A recent paper by Prinn et al. (2001) reports a strong positive trend of 15% ± 22% for the period 1979–1989 (or 1.3% $yr^{-1}$) followed by a strong decrease the following decade. At this point there is very little to add to their points of view. Our 'best' model simulation (S1) suggests that an increasing OH and decreasing turn-over time of methane during the period 1979–1993 as shown in Fig. 3, which is consistent with the results of Krol et al. (2001).

Another model uncertainty arises from the simplified way to treat the stratospheric methane sink. In this model version an annual amount varying between 38 and 42 Tg $yr^{-1}$ was destroyed in the upper 5 model levels in the stratosphere, which results were derived from a 2D model calculation by Bruhl and Crutzen (1994). In addition, stratospheric chlorine increased during the period 1979–1993, possibly influencing the stratospheric lifetime of methane. In this study the impact of this uncertainty is expected to be small, since chlorine accounts for only about 20% of the stratospheric $CH_4$ oxidation.

## 6. Conclusions

We used a set of multi-annual global 3D chemical transport model (CTM) simulations to check the consistency of changes in photochemistry, meteorology, methane sources

and sinks, and methane observations. The reference simulation yields a rather consistent picture of global methane sources and sinks. In this simulation we used annually varying meteorological fields derived from the ECMWF re-analysis for the years 1979–1993, annually varying $NO_x$, CO, and NMHC emissions (van Aardenne et al., 2001) and ozone column boundary conditions obtained from TOMS. The methane concentrations were adjusted in the boundary layer to a monthly and zonally averaged concentration field based on observations, with the observed global annual trend superimposed to this field. The amount of methane destroyed by photochemical reactions in the model and replenished into the lower model layers is therefore a good measure of the methane emissions needed to balance the observations.

Globally, during the period 1979–1993 the calculated tropospheric methane lifetime decreases from 9.2 to 8.9 years ($-0.26 \pm 0.06\%$ yr$^{-1}$). This is consistent with the work of Krol et al. (1998).

The calculated methane emissions trends are consistent with the time evolution of methane emissions from an independent database compiled by van Aardenne et al. (2001). For the period 1979–1993 this trend amounts to 2.7 Tg $CH_4$ yr$^{-1}$. The eruption of Mt. Pinatubo in 1991 may have lead to a strong decrease of methane emissions by about 13 Tg yr$^{-1}$. In the SH we find a small additional methane emissions increasing by 1 Tg yr$^{-1}$, however due to a lack of measurements this increase is very uncertain.

The calculated interannual variability of (natural) methane sources is of the order of 8 Tg $CH_4$. We showed in the Appendix that our method using a limited set of observations tends to give an underestimate of this variability by 15% globally and 40% in the NH. Sensitivity studies showed that in studies of methane inter-annual variability it is most important to include the variability of the oxidant fields, and to a lesser extent the transport variability.

The main uncertainty in this work is associated with the use of a limited set of measurements to derive global emissions and trends. The uncertainties associated with our method were evaluated using an synthetic emission dataset, which was used to 'generate' concentrations at the locations of the measurement stations. Using these

synthetic emissions we were able to calculate trends and variability with an accuracy of about 50%. The real-world accuracy is probably better. The order of magnitude of this uncertainty is similar to the more formal inversion techniques.

We hypothesized that most of the inter-annual variability would be related to mid- and low-latitude emissions from biomass burning or natural wetlands. Indeed, we found correlations between the variations in residual emissions and interannual variations in temperature. The correlations are rather weak and should thus be interpreted with great care. If the emission variability could be attributed completely to wetland emissions the emission sensitivity would be about 15% $K^{-1}$. To a lesser extent also biomass burning emissions could contribute to the variability. Studies that are better constrained by measurements are needed to further corrobate these findings. Finally, it is worthwhile to mention that we did not find significant correlations between a five-month running average of the residual natural emissions and the El Niño Southern Oscillation index.

## Appendix: Test with synthetic emissions

Our method can be seen as a rather informal inverse technique, similar to the more rigorous and formally more correct method described in, e.g. (Law and Simmonds, 1996). The largest uncertainty pertaining to our method is whether a prescribed zonal field for a single year modified with a trend derived from a limited set of measurements can be used to retrieve trends in emissions and to deduce variability. To evaluate this difficult problem, we generated a set of synthetic emissions, which consisted of the emission data-set evaluated by Houweling et al. (2000) supplemented with an artificial, but realistic trend of 1% $yr^{-1}$ for all anthropogenic emissions. In addition we applied an artificial variability on the biomass burning and wetland emissions, which are considered to be the main sources of inter-annual variability. We assumed a period of 2 and 4 years and amplitude of 33% and 25%, respectively. The variability of the synthetic emissions was on purpose chosen very high to provide a rigorous test for our method. In the next step



ACPD
2, 249–287, 2002

the monthly and zonal average field for 1987 was calculated, and the surface layer $CH_4$ concentrations at the locations of the NOAA sites were used to calculate an 1979–1993 trend. These zonal average concentrations and their trends were then used to 'nudge' the model. The further steps followed the same procedure as described before, using varying OH fields and varying meteorology. Shortly, the method tests to what extent the information contained in a limited amount of data can be used to retrieve relatively variable and complex emissions. Figure 8 shows the annual average original synthetic and recalculated emissions. The corresponding statistical parameters are presented in Table 6. Overall, variability and trend are indeed recovered using the method, and high correlation is found between the prescribed and re-calculated emissions. However, except for the southernmost region, the retrieved variability is 20–30% less than the prescribed ones, due to the use of the 'background' station data, and the associated loss of information. The calculated trends are associated with an uncertainty of about 50%.

The largest obvious deviation is found in the region 45 S–90 S, where spurious emissions are calculated. However, the maximum deviation of the retrieved and synthetic emissions is of similar magnitude (about 10 Tg $yr^{-1}$) as in other regions. Interestingly, the emissions calculated using 'real' measurements show much more variability than in this synthetic case. We think this is due to the fact that the 'real' yearly emission variations are smaller, and that therefore the annual trends and 2D $CH_4$ fields are more representative for the 'real' situation. It is therefore quite likely that the trend of $CH_4$ can be retrieved with a substantially better accuracy than 50% .

## References

Barbosa, P. M., Stroppiana, D., Gregoire, J.-M., and Cardosa Pereira, J. M.: An assessment of vegetation fire in Africa (1981–1991): Burned areas, burned biomass, and atmospheric emissions, Global Biogeochem. Cycles, 13, 933–950, 1999. 265

Bekki, S., Law, K. S., and Pyle, J. A.: Effect of ozone depletion on atmospheric $CH_4$ and CO concentrations, Nature, 371, 595–597, 1994. 251

Bruhl, C. and Crutzen, P. J.: MPIC two dimensional model, NASA Ref. Publ., 1292, 103–104, 1993. 255, 266

Dentener, F. J. and Crutzen, P. J.: A global 3D Model of the ammonia cycle, J. Atmos. Chem. 19, 331–369, 1994. 254

Dentener, F., Feichter, J., and Jeuken, A.: Simulation of the transport of Radon$^{222}$ using on-line and off-line global models at different horizontal resolutions: a detailed comparison with measurements, Tellus, 51B, 573–602, 1999. 254

Dlugokencky, E. J., Masarie, K. A., Lang, P. M., and Tans, J. P.: Continuing decline in the growth rate of the atmospheric methane burden, Nature, 393, 447–450, 1998. 251, 252

Etheridge, D. M., Steele, L. P., Francy, R. J., and Langenfels, R. L.: Atmospheric methane between 1000 A.D. and present: Evidence of anthropogenic emissions and climatic variability, J. Geophys. Res., 103, 15 797–15 993, 1998. 257

Fortuin, P. and Kelder, H.: An ozone climatology based on ozone sonde and satellite measurements, J. Geophys. Res., 103, 31 709–31 734, 1998. 254

Fung I., John, J., Lerner, J., Matthews, E., Prather, M., Steele, L. P., and Fraser, P. J.: Three-dimensional model synthesis of the global methane cycle, J. Geophys. Res., 13 033–13 065, 1991. 252, 253

Ganzeveld, L. N., Roelofs, G. J., and Lelieveld, J.: A dry deposition parameterization for sulfur oxides in a chemistry and general circulation model, J. Geophys. Res., 103, 5679–5694, 1998. 254

Gibson, R., Kallberg, P., and Uppsala, S.: The ECMWF re-analysis (ERA) project, ECMWF Newsletter, 73, 7–11, 1997. 253

Guelle, W., Balkanski, Y. J., Schulz, M., Dulac, F., and Monfray, P.: Wet deposition in a global size-dependent aerosol transport model, 1, Comparison of a 1 year $Pb^{210}$ simulation with ground measurements, J. Geophys. Res., 103, 11 429–11 445, 1998. 254

Gupta, M. L., Cicerone, R. J., and Elliot, S.: Perturbation to global tropospheric oxidizing capacity due to latitudinal redistribution of surface sources of $NO_x$, $CH_4$, and CO, Geophys. Res. Let., 21, 3931–3934, 1998. 261, 265

Hein, R., Crutzen, P. J., and Heimann, M.: An inverse modeling approach to investigate the global atmospheric methane cycle, Global Biogeochem. Cycles, 11, 43–76, 1997. 252, 253, 257, 265

Heimann, M.: The global atmospheric tracer model TM2, Technical report no. 10, Deutsches Klimarechenzentrum (DKRZ), Hamburg, Germany, 1995. 253

Hogan, K. B. and Harriss, R. C.: Comment on 'A dramatic decrease in the growth rate of atmospheric methane in the northern hemisphere during 1992' by Dlugokencky, et al., Geophys. Res. Lett., 21, 2445–2446., 1994. 251

Houweling S., Dentener, F. J., Lelieveld, J., Walter, B., and Dlugokencky,E. J.: The modeling of tropospheric methane; how well can point measurements be reproduced by a global model?, J. Geophys. Res., 105, 8981–9002, 2000. 252, 253, 256, 259, 261, 264, 265, 268

Houweling S., Kaminski, T., Dentener, F., Lelieveld, J., and Heimann, M.: Inverse modelling of methane sources and sinks using the adjoint of a global transport model, J. Geophys. Res., 104, 26 137–26 160, 1999. 251, 252, 255, 258, 260, 274

Houweling S., Dentener, F., and Lelieveld, J.: The impact of nonmethane hydrocarbon compounds on tropospheric photochemistry, J. Geophys. Res., 103, 10 673–10 696, 1998. 253, 254, 255

Karlsdottir, S., Isaksen, I. S. A., Myhre, G., and Berntsen, T. K.: Trend analysis of $O_3$ and CO in the period 1980–1996: A three-dimensional model study, J. Geophys. Res., 105, 28 907–28 933, 2000. 252

Krol, M. C., Van Leeuwen, P. J., and Lelieveld, J.: Global OH trend inferred from methylchloroform measurement, J. Geophys. Res., 103, 10 697–10 711, 1998. 252, 261, 267

Krol, M. C., Van Leeuwen, P. J., and Lelieveld, J.: Reply to the comment of Prinn and Huang on "Global OH trend inferred from methylchloroform measurements" by Krol, M., et al. 1998, J. Geophys. Res, 23 159–23 164, 2001. 252, 266

Krol, M. and van Weele, M.: Implication of variation of photodissociation rates for global atmospheric chemistry, Atmos. Environ., 31, 1257–1273, 1997. 254

Landgraf, J. and Crutzen, P. J.: An efficient method for online calculations of photolysis and heating rates, J. Atmos. Science, 55, 863–878, 1998. 254

Lassey, K. R., Lowe, D. C., Brenninkmeyer, C. A. M., and Gomez, A. J.: Atmospheric methane and its carbon isotopes in the Southern Hemisphere: their time series and an instructive model, Chemosphere, 26, 95–109, 1993. 253

Law, R. and Simmonds, I.: The sensitivity of deduced $CO_2$ sources, and sinks to variations in transport and imposed surface concentrations, Tellus B, 613–625, 1996. 268

Lelieveld, J., Crutzen, P. J., and Dentener, F. J.: Changing Concentration, lifetime and climate forcing of atmospheric methane, Tellus, 50B, 128–150, 1998. 251, 252

Lelieveld, J. and Dentener, F.: What controls Tropospheric Ozone?, J. Geophys. Res., 3531–3551, 2000. 251, 253, 254, 259

Louis, J. F.: A parametric model of vertical eddy fluxes in the atmosphere, Boundary Layer Met., 17, 187–202, 1979. 254

Marland, G., Boden, T. A., and Andres, R. J.: Global, regional, and national $CO_2$ emissions. Trends: A compendium of data on Global Change, Carbon Dioxide Analysis Center, Oak Ridge National Laboratory, U.S. Department of Energy, Oak Ridge, Tenn., USA, 2000. 255

Marufu, L., Dentener, F., Lelieveld, J., Andreae, M. O., and Helas, G.: Photochemistry of the African Troposphere: the influence of biomass burning emissions, J. Geophys. Res., 14 513–14 530, 2000. 265

McCulloch, A. and Midgley, P. M.: The production and global distribution of emissions of trichloroethane and dichloromethane over the period 1988–1992, Atmos. Environ, 30, 601–608, 1996. 265

McPeters, R. D., Bhartia, P. K., Krueger, A. J., Herman, J. R., Schlesinger, B., Wellemeyer, C. G., Seftor, C. J., Jaross, G., Taylor, S. L., Swissler, T., Torres, O., Labow, G., Byerly, W., and Cebula, R. P.: Nimbus-7 Total Ozone Mapping Spectrometer (TOMS) Data Products User's Guide, NASA Reference Publication 1384, Washington D. C., 1996.

Olivier, J. G. J., Bouwman, A. F., Berdowski, J. J. M., Veldt, C., Bloos, J. P. J., Visschedijk, A. J. H., van der Maas, C. W.M., and Zandveld, P. Y. J.: Sectoral Emission inventories of greenhouse gases on a per country basis as well as 1 × 1, Env. Sci. Policy, 2, 241–263, 1999. 255

Peters, W., Krol, M., Dentener, F., and Lelieveld J.: Identification of an ENSO signal in a multi-year global simulation of tropospheric ozone, J. Geophys. Res., 106, 10 389–10 402, 2001. 259

Prather, M., Ehhalt, D., Dentener, F., Derwent, R., Dlugokencky, E., Holland, E., Isaksen, I., Katima, J., Kirchhoff, V., Matson, P., Midgley, P., and Wang, M.: Atmospheric chemistry and greenhouse gases, Chapter 4, in: Climate Change 2001, The scientific basis: Contribution of working group I to the Third assessment report of the Intergovernmental Panel on Climate, (Eds) Houghton, J. T., Ding, Y., Griggs, D. J., Noguer, M., van der Linden, P. J., Dai, X., Maskell, K., and Johnson, C. A., Cambridge University Press, Cambridge, UK and New York, NY, USA, p. 881, 2001. 250, 251, 252, 260

Prinn, R. G., Weiss, R. F., Miller, B. R., Huang, J., Alya, F. N., Cunnold, D. M., Fraser, P. J., Hartley, D. E., and Simmonds, P. G.: Atmospheric trends and lifetime of $CH_3CCl_3$ and global

OH concentrations, Science, 269, 187–190, 1995. 252, 264
Prinn, R. G., Huang J., Weiss, R. F., Cunnold, D. M., Fraser, P. J., Simmonds, P. G., McCulloch, A., Harth, C., Salameh, P., O'Doherty S., Wang, R. H. J., Porter, L., and Miller, B. R.: Evidence for substantial variations of atmospheric hydroxyl radicals in the past two decades, Sience, 292, 1882–1888, 2001. 252, 266
Prinn, R. G. and Huang J.: Comment on "Global OH trend inferred from methylchloroform measurements by Krol, M., et al., 1998", J. Geophys. Res., 23 151–23 157, 2001. 252, 266
Russel, G. and Lerner, J.: A new finite difference scheme for the tracer transport equation, J. Appl. Meteorol., 20, 1483–1498, 1981. 254
Sander, S. P., Friedl, R. R., DeMore, W. B., Kurylo, M. J, Hampson, R. F., Huie, R. E., Moortgat, G. K., Ravishankara, A. R., Kolb C. E., and Molina, M. J.: Chemical Kinetics and Photochemical Data for Use in Stratospheric Modeling, Evaluation 13, JPL publication, 00-003, Jet Propulsion Laboratory, California, USA, 2000. 264
Tiedtke, M.: A comprehensive mass-flux scheme for cumulus parameterization in large-scale models, Mon. Weather Rev., 117, 1779–1800, 1989. 254
Van Aardenne, J. A., Dentener, F. J., Klein Goldewijk, C. G. M., Lelieveld, J., and Olivier, J. G. J.: A high resolution data set of historical anthropogenic trace gas emissions for the period 1890–1990, Global. Biogeochem. Cycles, 15, 909–928, 2001. 255, 256, 258, 261, 263, 267
Walter, B. P. and Heimann, M.: A process-based, climate sensitive model to derive methane emissions from natural wetlands: Application to five wetland sites, sensitivity to model parameters, and climate, Global Biogeochem. Cycles, 14, 745–765, 2000. 263
Wild, O. and Prather, M.: Excitation of the primary tropospheric chemical mode in a global three-dimensional model, J. Geophys. Res., 105, 24 647–24 660, 2000. 260
Ziemke, J., Chandra, S., and Bartia, P.: Seasonal and interannual variabilities in tropical tropospheric ozone, J. Geophys. Res., 104, 21 245–21 442, 1999. 259

**Table 1.** Emissions Tg $CH_4$ $yr^{-1}$ evaluated by Houweling et al. (1999) used as an a priori estimate

| region | 90 N–45 N | 45 N–0 N | 0 S–45 S | 45 S–90 S | Global |
|---|---|---|---|---|---|
| coal mining | 13.5 | 22.1 | 2.4 | 0.0 | 38.0 |
| soil oxidation | −13.3 | −10.6 | −6.0 | −0.1 | −30.0 |
| wild animals | 1.4 | 1.9 | 1.7 | 0.0 | 5.0 |
| domestic ruminants | 21.4 | 51.9 | 19.1 | 0.6 | 93.0 |
| oceans | 5.0 | 4.9 | 3.9 | 1.2 | 15.0 |
| termites | 1.9 | 9.6 | 8.5 | 0.0 | 20.0 |
| fossil+domestic fuel | 2.3 | 14.9 | 2.9 | 0.0 | 20.0 |
| gas production | 24.3 | 24.7 | 2.0 | 0.1 | 51.0 |
| vulcanoes | 0.0 | 2.2 | 1.3 | 0.0 | 3.5 |
| biomass burning | 0.0 | 19.5 | 22.5 | 0.0 | 42.0 |
| permafrost | 1.0 | 0.0 | 0.0 | 0.0 | 1.0 |
| landfills | 11.5 | 31.6 | 4.8 | 0.0 | 48.0 |
| rice | 0.5 | 69.8 | 9.7 | 0.0 | 80.0 |
| wetlands | 31.4 | 48.4 | 65.1 | 0.0 | 145.0 |
| sum natural | 27.4 | 56.4 | 74.5 | 1.2 | 159.5 |
| sum anthropogenic | 73.4 | 234.5 | 63.4 | 0.7 | 372.0 |



ACPD
2, 249–287, 2002

**Table 2.** NOAA stations used in this work to derive the model trends

| Station | Code | Long | Lat |
|---|---|---|---|
| Polar Front | CTN | 2 E | 66 N |
| Cold Bay | CBA | 162 W | 55 N |
| Mould Bay | MBC | 119 W | 76 N |
| Barrow | BRW | 156 W | 71 N |
| Key Biscayne | KEY | 80 W | 25 W |
| Mauna Loa | MLO | 155 W | 19 N |
| Cape Kumukahi | KUM | 154 W | 19 N |
| Guam | GMI | 144 E | 13 N |
| Ascension Island | ASC | 14 W | 8 S |
| Tutuila | SMO | 170 W | 14 S |
| South Pole | SPO | 24 W | 90 S |

**Table 3.** Lifetime and trend of $CH_4$ lifetime for the period 1979–1993. Lifetime is calculated for the year 1979 considering a tropopause height of 100 hPa

| Region | Trend [% $yr^{-1}$] | Uncertainty of trend [% $yr^{-1}$] | Tropospheric lifetime [year] |
|---|---|---|---|
| 90 N–45 N | −0.23 | 0.20 | 28 |
| 45 N–EQ | −0.25 | 0.07 | 6.5 |
| EQ–45 S | −0.27 | 0.07 | 7.5 |
| 45 S–90 S | −0.36 | 0.15 | 55 |
| Global | −0.26 | 0.06 | 9.2 |



ACPD
2, 249–287, 2002

**Table 4.** Standard deviation of residual emissions (as a measure of variability), trend and uncertainty of this trend for the period 1979–1993. The trend is also calculated for a shorter period 1979–1991. Units are [Tg $CH_4$ $yr^{-1}$]

| Region | Standard deviation | Trend 1979–1993 | Uncertainty of trend | Trend 1979-1993 | Uncertainty of trend |
|---|---|---|---|---|---|
| 90 N–45 N | 1.6 | 0.14 | 0.09 | 0.09 | 0.12 |
| 45 N–0 N | 5.2 | −0.64 | 0.27 | −0.17 | 0.24 |
| EQ–45 S | 3.7 | 0.49 | 0.18 | 0.80 | 0.17 |
| 45 S–90 S | 1.1 | 0.16 | 0.05 | 0.24 | 0.09 |
| Global | 7.8 | 0.16 | 0.48 | 0.98 | 0.43 |



ACPD
2, 249–287, 2002

**Table 5.** Correlation coefficient $r$ of residual emissions based on the period 1979–1993. Correlation coefficients larger than 0.45 are marked with an asterisk

| region | 90 N–45 N | 45 N–0 N | 0 S–45 S | 45 S–90 S | global |
|---|---|---|---|---|---|
| CANADA | 0.197 | −0.112 | 0.080 | 0.046 | 0.007 |
| USA | 0.145 | −0.231 | 0.309 | 0.186 | 0.045 |
| LATIN AMERICA | −0.107 | −0.126 | −0.074 | −0.228 | −0.177 |
| AFRICA | −0.112 | 0.024 | 0.630* | 0.498* | 0.356 |
| OECD EUROPE | 0.100 | 0.339 | 0.514* | 0.509* | 0.523* |
| EASTERN EUROPE | 0.135 | 0.432 | 0.301 | 0.250 | 0.488* |
| FORMER USSR | 0.438 | 0.221 | 0.160 | 0.147 | 0.333 |
| MIDDLE EAST | −0.303 | 0.250 | 0.148 | 0.142 | 0.195 |
| INDIA | −0.270 | −0.306 | 0.347 | 0.308 | −0.055 |
| CHINA | −0.144 | −0.160 | 0.450* | 0.311 | 0.113 |
| EAST ASIA | 0.096 | 0.090 | 0.611* | 0.560* | 0.441 |
| OCEANIA | −0.369 | 0.271 | −0.095 | −0.137 | 0.035 |
| JAPAN | −0.099 | −0.059 | 0.489* | 0.403 | 0.225 |

**Table 6.** Statistical analysis of the synthetic (S) emissions, and the retrieved (R) emissions [Tg $CH_4$ $yr^{-1}$]. The standard deviation (sd) is a measure of the inter-annual variability. The trend is associated with a calculated uncertainty (trend unc.) Correlation coefficient $r^2$ calculated using annual values of S and R.

| Region | $r^2$ | mean S | mean R | trend S | trend R | trend unc. S | trend unc. R | sd S | sd R |
|---|---|---|---|---|---|---|---|---|---|
| 90 N–45 N | 0.72 | 99.3 | 97.9 | 1.00 | 0.68 | 0.34 | 0.17 | 7.1 | 4.1 |
| 45 N–0 N | 0.87 | 286.1 | 276.4 | 3.10 | 2.02 | 0.59 | 0.48 | 16.9 | 11.9 |
| EQ–45 S | 0.62 | 135.2 | 136.1 | 0.76 | 1.48 | 0.78 | 0.52 | 13.1 | 10.8 |
| 45 S–90 S | 0.34 | 1.9 | 5.9 | 0.00 | 0.39 | 0.00 | 0.18 | 0.04 | 3.33 |
| Global | 0.84 | 522.6 | 516.3 | 4.88 | 4.58 | 1.70 | 1.32 | 35.0 | 29.6 |



ACPD
2, 249–287, 2002

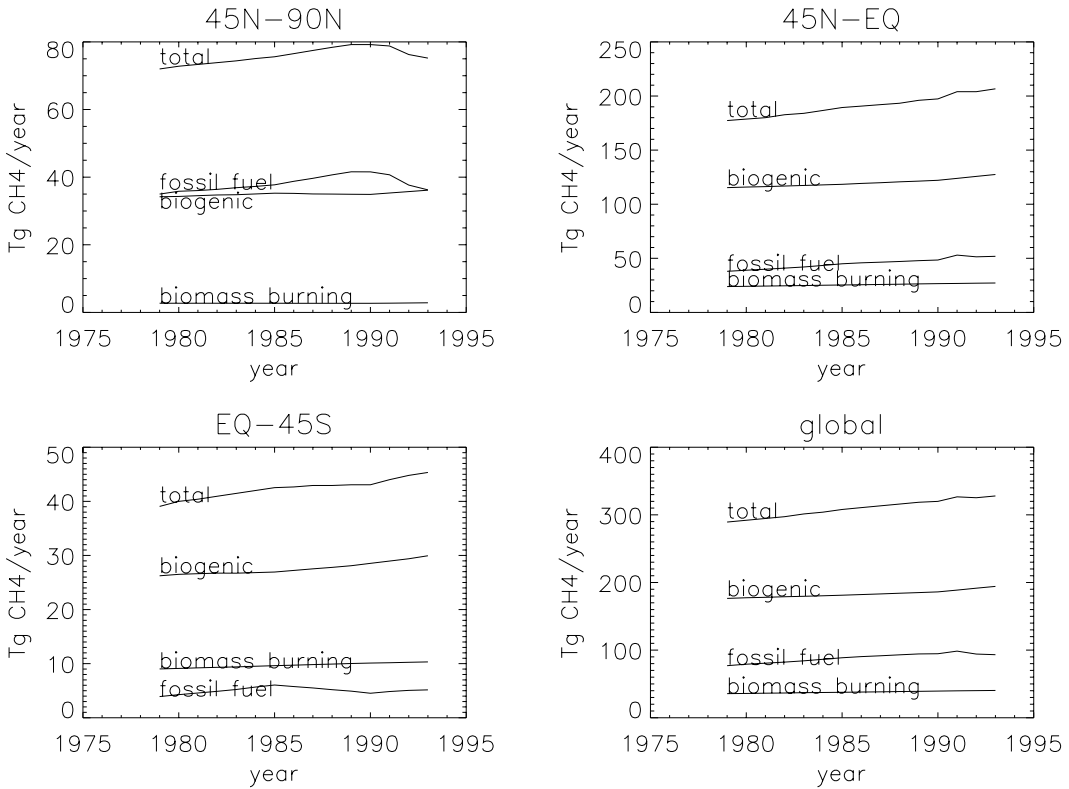


**Fig. 1.** Temporal development of anthropogenic emissions separated for biogenic, fossil fuel related, and biomass burning emissions. Global and 3 world regions.



ACPD
2, 249–287, 2002

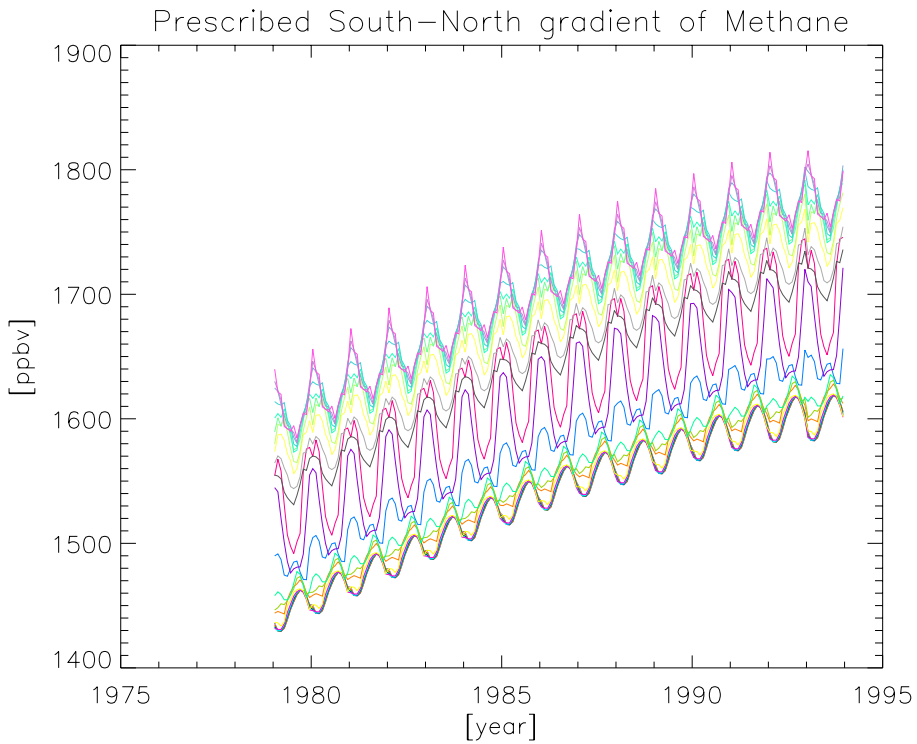


**Fig. 2.** Latitudinal and temporal evolution of prescribed methane volume mixing ratio [ppbv]. Each color represents a different latitude, starting from 86 N at the top in steps of 8 degrees.



**ACPD**

2, 249–287, 2002

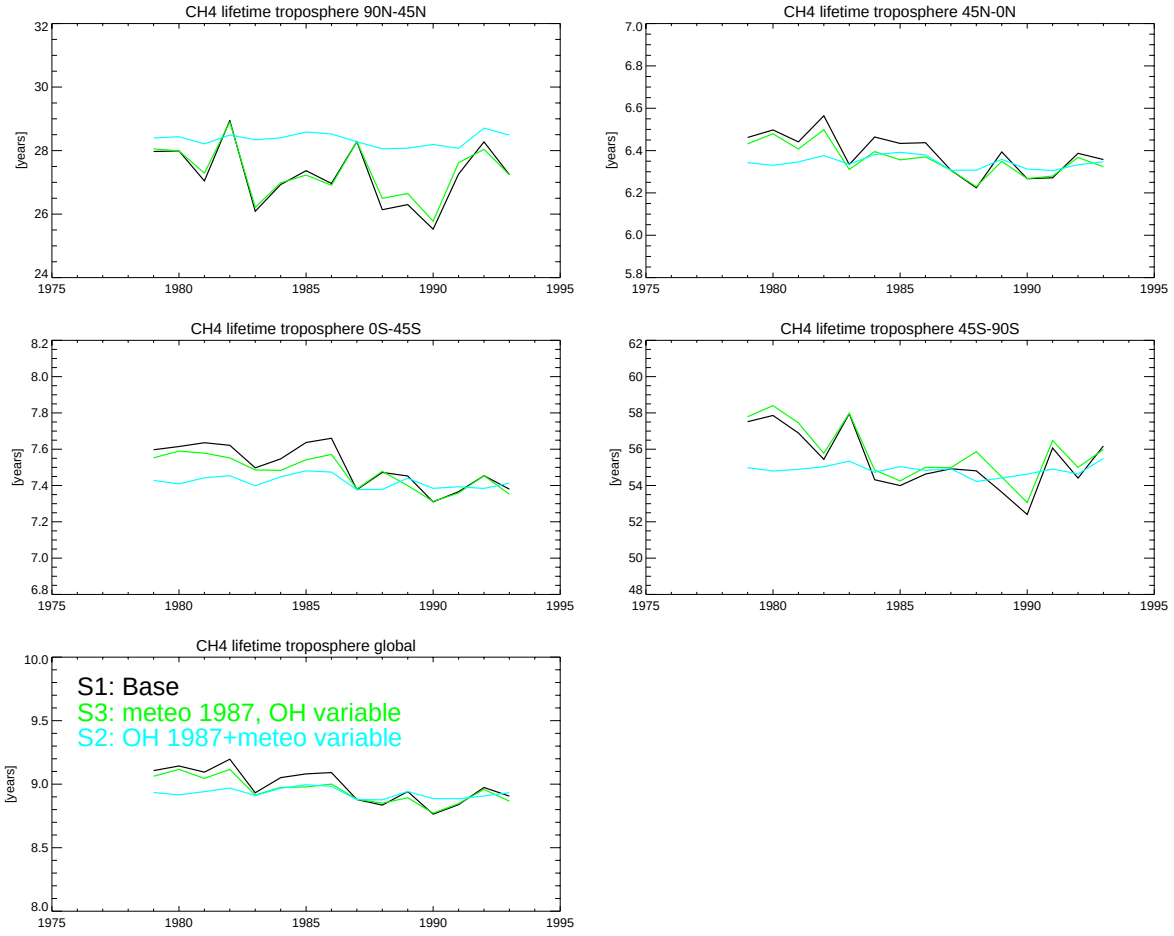


**Fig. 3.** Methane lifetime [years] determined for 3 simulations, for the 4 regions and global



ACPD
2, 249–287, 2002

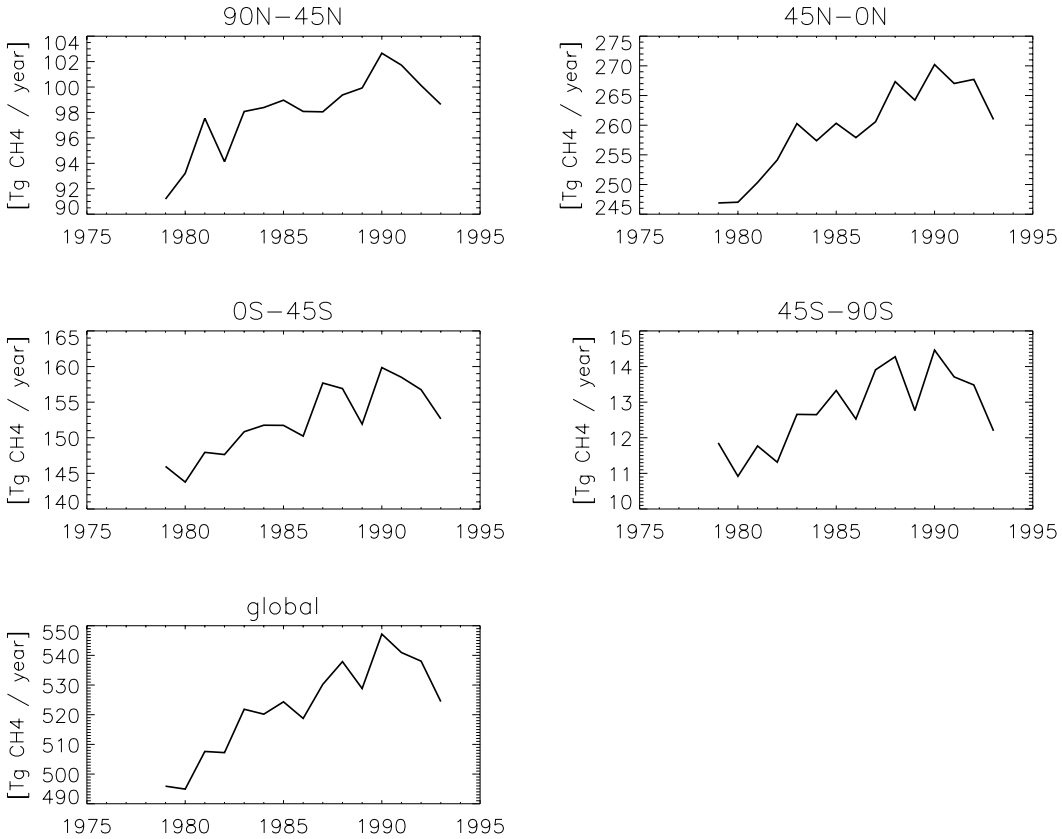


**Fig. 4.** Calculated emissions [Tg $CH_4$ $yr^{-1}$] for the years 1979–1993.



ACPD
2, 249–287, 2002

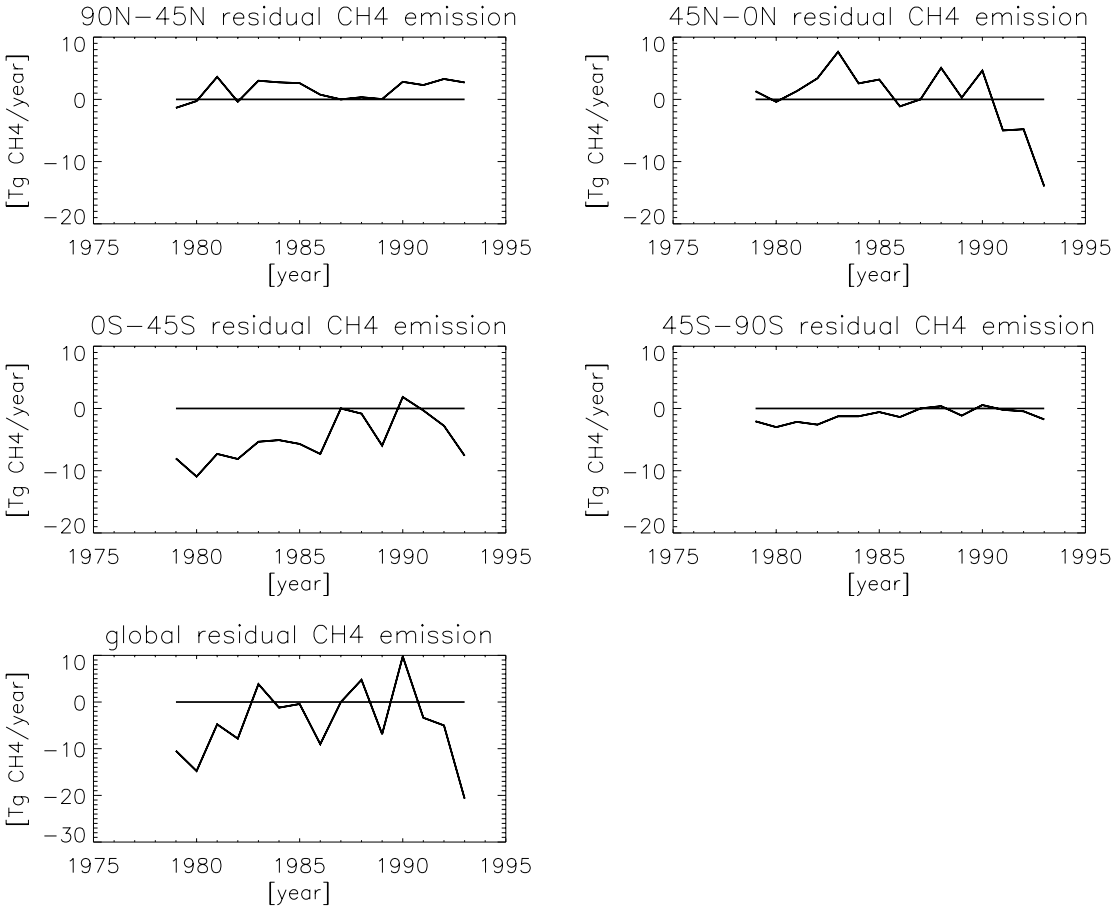


**Fig. 5.** Residual emissions [Tg $CH_4$ $yr^{-1}$] for the base case and the 4 regions, calculated according to Eq. (3).



**ACPD**

2, 249–287, 2002

**Trends and inter-annual variability of methane emissions**

F. Dentener et al.

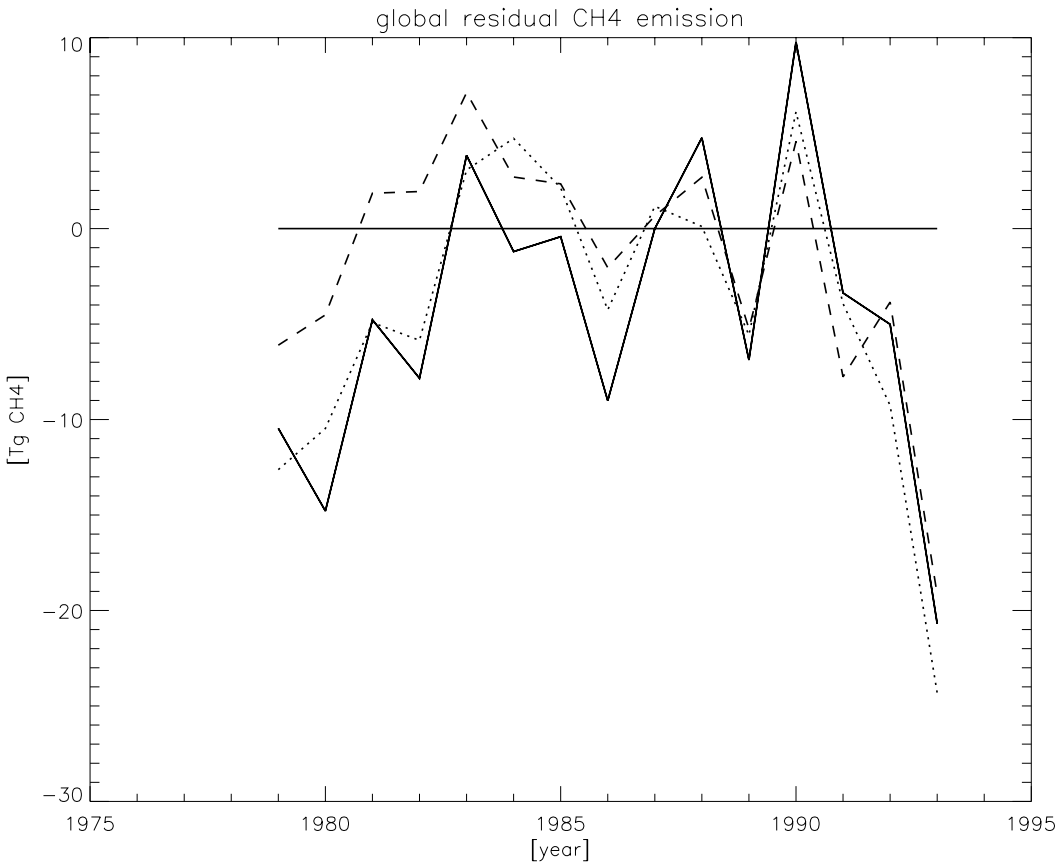


**Fig. 6.** Global residual emissions [Tg $CH_4$ $yr^{-1}$] for the 3 case studies. Full line: S1 base simulation. Dashed line: S2 varying meteorology, constant OH. Dotted line: S3 varying OH, constant meteorology.



**ACPD**

2, 249–287, 2002

**Trends and inter-annual variability of methane emissions**

F. Dentener et al.

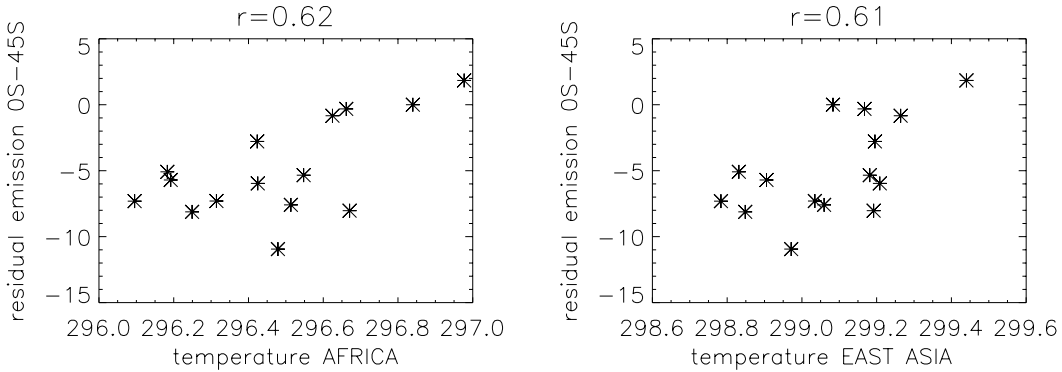


**Fig. 7.** Correlation of the residual emissions in the regions 0–45 S and temperature in Africa and S. E. Asia.



ACPD
2, 249–287, 2002

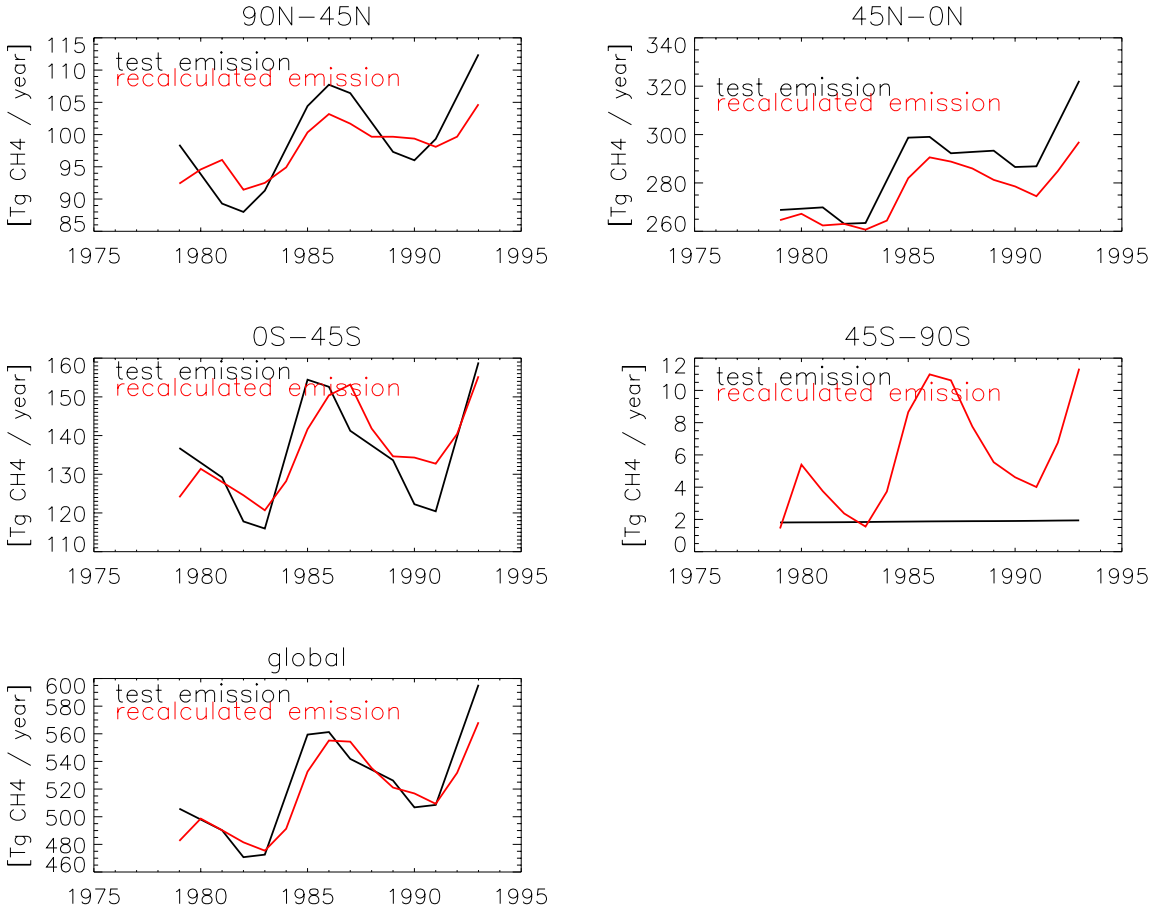


**Fig. 8.** Synthetic emission data set, and re-calculated emissions using a limited amount of station data.



ACPD
2, 249–287, 2002